Supplementary Figure 1

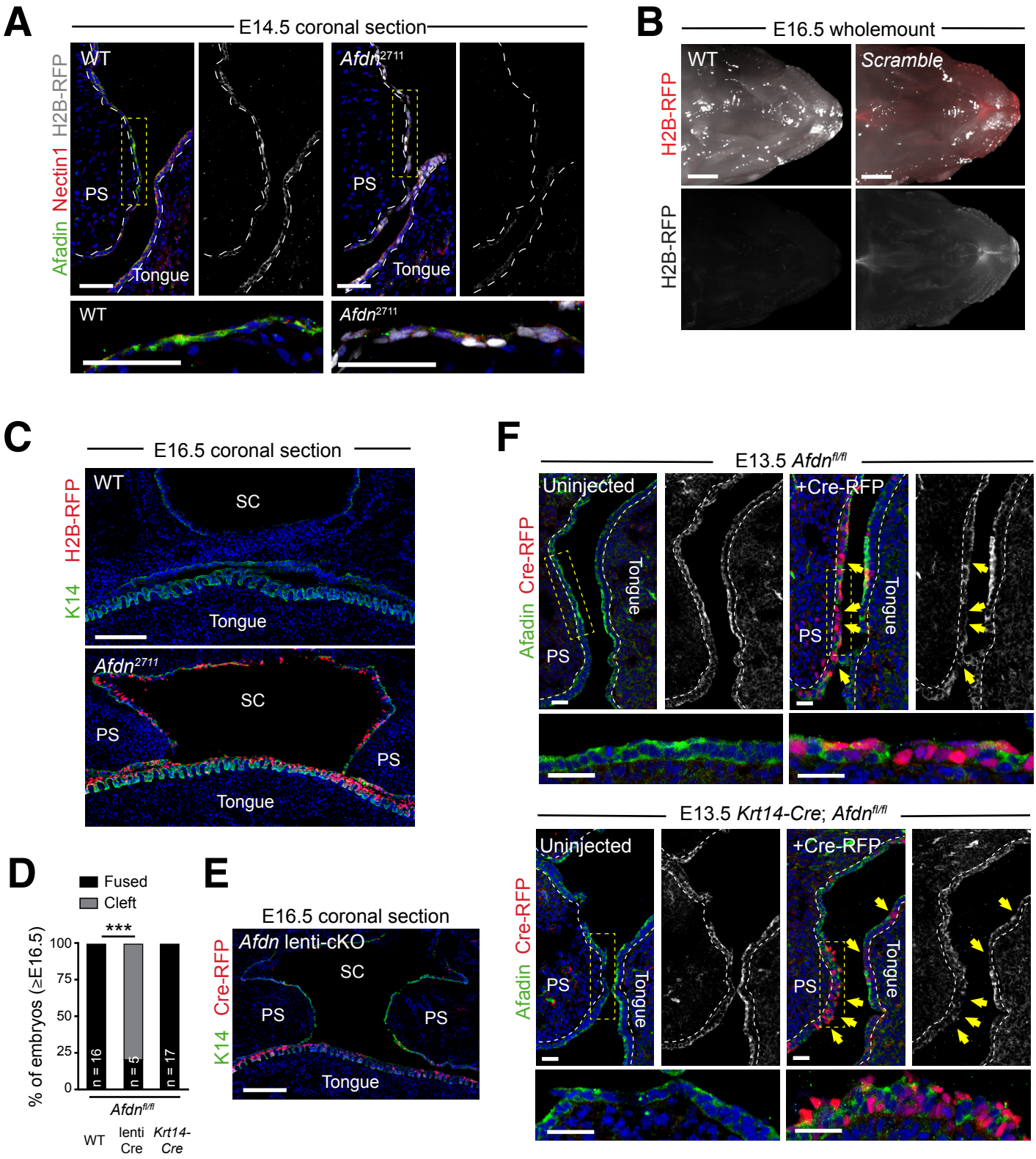

Figure S1 | Validation of transgenic models highlights improved efficacy of LUGGIGE

(A) E14.5 coronal sections of WT (left) and *Afdn*^{2711} (right) PS immunostained with Afadin (green), nectin-1 (red) and H2B-RFP (grey), demonstrating effective loss of Afadin accumulation in transduced epithelia; high magnification images of boxed region are shown in grayscale below. (B) Darkfield (top) and fluorescent (bottom) stereoscope images of E16.5 *Scramble H2B-RFP* infected embryo and uninjected littermate. H2B-RFP (red) is overlaid in the top panel. (C) Immunofluorescent image of E16.5 *Afdn*^{2711} and WT oral cavity. Some *Afdn*^{2711} embryos display normal PS elevation but fail to approximate. (D) Rate of CP phenotypes at E16.5 in *Afdn*$^{fl/fl}$ controls, *Afdn*$^{fl/fl}$ lenti-Cre, and *Afdn*$^{fl/fl}$ K14-Cre knockout littermates. *Afdn* knockout via lenti-Cre is suffient to cause CP, while K14-Cre is insufficient. (E) Immunofluorescent image of E16.5 *Afdn*$^{fl/fl}$ lenti-Cre oral cavity, demonstrating CP. (F) (Top) E13.5 *Afdn*$^{fl/fl}$ PS including Cre-RFP injected (right) and uninjected (left) samples stained for Afadin (green; grey isolated channel) and Cre-RFP (red). LUGGIGE-mediated recombination results in efficient loss of Afadin accumulation by E13.5. (Bottom) E13.5 *Krt14-Cre; Afdn*$^{fl/fl}$ PS including Cre-RFP injected (right) and uninjected (left) samples stained for Afadin (green; grey isolated channel) and Cre-RFP (red). While *Krt14-Cre; Afdn*$^{fl/fl}$ embryos still display robust Afadin signal (compared to uninjected *Afdn*$^{fl/fl}$ PS in Fig. S1C), addition of Cre-RFP results in mosaic loss of Afadin accumulation in transduced epithelia. High magnification images of boxed regions are shown below. Scale bars 50 μm (A), 1 mm (B), 200 μm (C,E), 25 μm (F). *** $P <$ 0.001, by Fisher's exact test.

Supplementary Figure 2

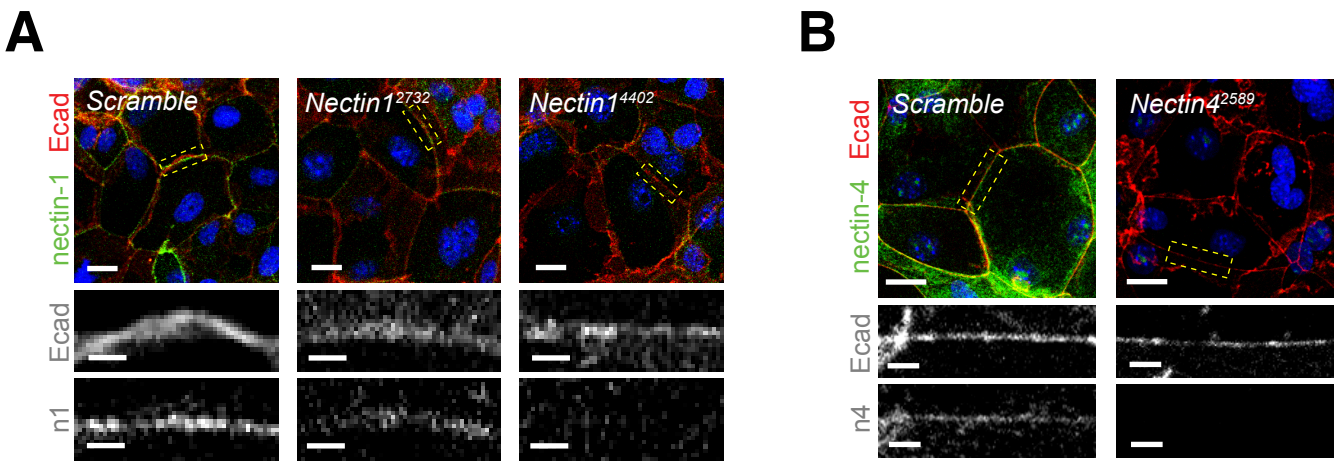

Figure S2 | *In vitro* validation of Nectin1/4 shRNA efficacy using calcium-shift assays

(A) Primary mouse keratinocytes after 8h Ca^{2+} shift—labeled with E-cad (red) and nectin-1 (green)—which accumulate in linear bands at cell-cell junctions. Yellow boxed region shown at high magnification below. *Nectin1*$_{4402}$ knockdown cells show robust loss of nectin-1, while *Nectin1*$_{2732}$ cells show intermediate loss compared to *Scramble* controls. (B) 8h Ca^{2+}-shifted keratinocytes stained for nectin-4 (green) and E-cad (red). *Nectin4*$_{2589}$ knockdown cells show robust loss of nectin-4 protein at cell-cell junctions. Scale bars 20 μm (large), 5 μm (zoom).

Supplementary Figure 3

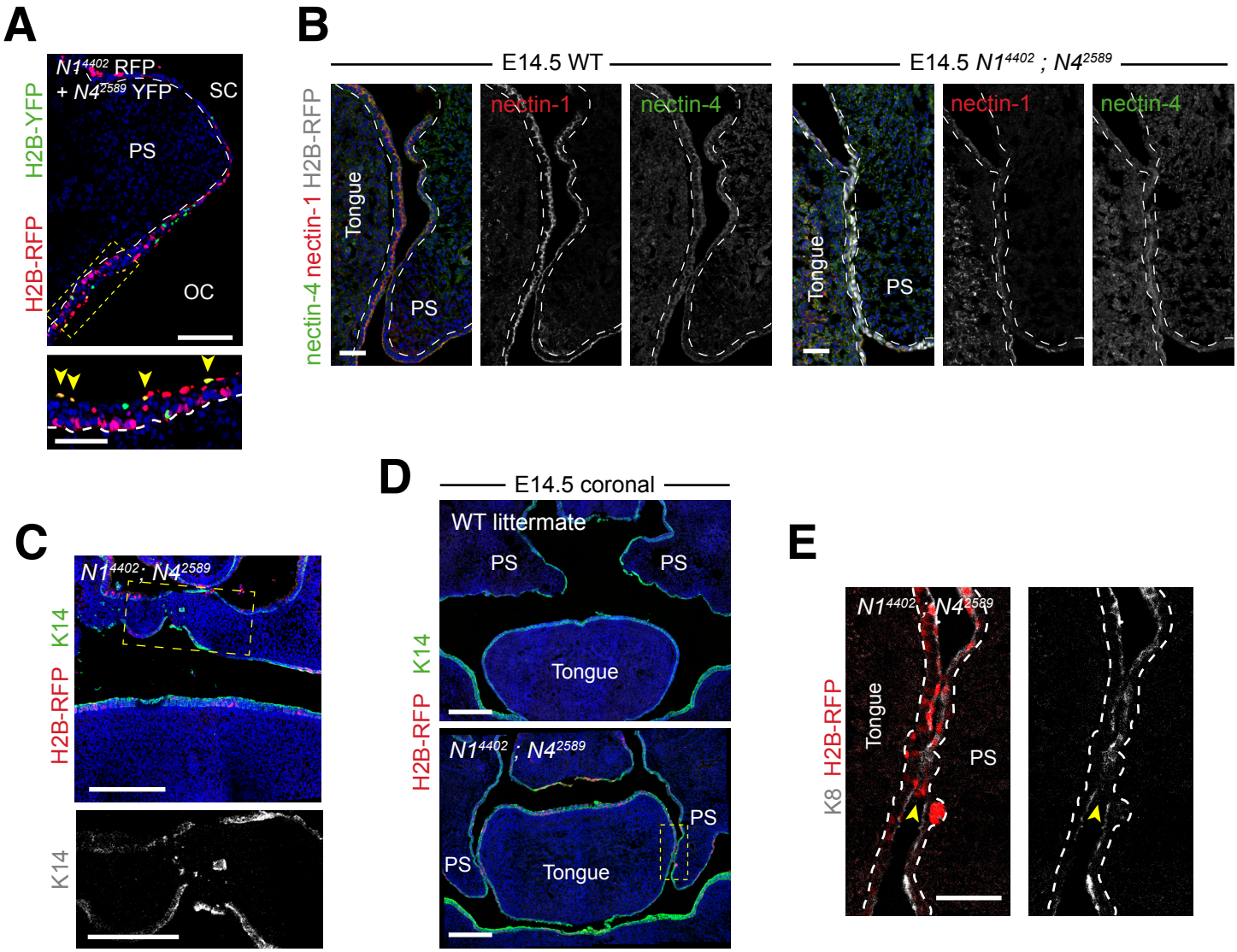

Figure S3 | Dual loss of *Nectin1* and *Nectin4* in a novel, double shRNA construct delays PS elevation and can result in residual MES.

(A) E16.5 coronal sections of *Nectin1*$_{4402}$ H2B-RFP/*Nectin4*$_{2589}$ H2B-YFP PS immunostained with GFP (green) and mCherry (red), demonstrating rare dual-transduced cells (yellow arrows in high magnification image of boxed region, below). (B) Immunofluorescent image of E14.5 *Nectin1*$_{4402}$;*Nectin4*$_{2589}$ and WT PS stained with nectin-1 (red), nectin-4 (green) and H2B-RFP. Cells transduced with the double shRNA construct show efficient loss of both nectin-1 and nectin-4. (C) E16.5 *Nectin1*$_{4402}$;*Nectin4*$_{2589}$ oral cavity immunostained for K14 (green) and H2B-RFP (red) showing K14+ epithelia within the palatal mesenchyme. Zoomed region (greyscale K14 image) highlighted by yellow dashed box above. (D) Immunofluorescent image of E14.5 *Nectin1*$_{4402}$;*Nectin4*$_{2589}$ and WT littermate demonstrating delays in PS elevation. (E) Zoom of yellow boxed region in (D) showing direct contact between transduced H2B-RFP+ (red) cells of the PS and lateral tongue with gap in K8+ (grey) periderm layer, suggesting possible intraoral adhesion. Scale bars 100 μm (A), 50μm (B,E), 1 mm (C; large), 0.5 mm (C; zoom), 200 μm (D).* $P < 0.05$, ** $P < 0.01$, *** $P < 0.001$, by Fisher's exact test.